Journal of the Physical Society of Japan
Vol. 68, No. 2, February, 1999, pp. 561–566

Numerical Study of Impurity Scattering in Carbon Nanotubes

Takeshi NAKANISHI and Tsuneya ANDO[1]

The Institute of Physical and Chemical Research (RIKEN)
2–1 Hirosawa, Wako-shi, Saitama 351-0198

[1] *Institute for Solid State Physics, University of Tokyo*
7–22–1 Minato-ku, Roppongi, Tokyo 106-8666

(Received July 23, 1998)

The transmission and reflection coefficients of a carbon nanotube with a scatterer are calculated in a tight-binding model. The result obtained in a $\boldsymbol{k}\cdot\boldsymbol{p}$ scheme is shown to be essentially valid, including the complete absence of back scattering for scatterers with range larger than the lattice constant, unless the strength of the potential becomes comparable to the band width. When the potential strength is comparable to the band width, a resonant enhancement of back scattering appears and the result becomes completely different from that in the $\boldsymbol{k}\cdot\boldsymbol{p}$ scheme.

KEYWORDS: graphite, carbon nanotube, fullerene tube, impurity scattering, recursive Green's function technique

§1. Introduction

A carbon nanotube (CN) is a new quantum wire consisting of rolled graphite sheets.[1)] Because the distance between adjacent sheets is much larger than the distance between the nearest neighbor carbon atoms, electronic properties of CN's are determined essentially by those of a single-wall CN. A single-wall CN has also been synthesized.[2,3)] The purpose of this paper is to study impurity scattering in metallic single-wall CN in a tight-binding model.

Transport properties of CN's are interesting because of their unique topological structure. There have been some reports on experimental study of transport in CN bundles.[4)] Measurements of magnetotransport of a single nanotube became possible.[5,6)] Recently transport of a single-wall CN was observed,[7–9)] where experiments show large charging effects due to nonideal contacts or bending defects. Tunneling probabilities of a finite-length CN[10)] and a connection of different CN's[11–15)] were calculated. The conductivity was calculated also in a constant-relaxation-time approximation in the absence of a magnetic field.[16)] The magnetoconductivity was calculated using the Boltzmann transport equation[17)] and in a transmission approach[18)] for a model of short-range scatterers. The results were shown to have a close connection with transport in a two-dimensional graphite sheet.[19)]

In a previous paper,[20)] effects of impurity scattering in CN's were studied in detail and a possibility of complete absence of back scattering was predicted and proved rigorously except for scatterers having a potential range smaller than the lattice constant. This intriguing fact was related to Berry's phase acquired by a rotation in the wave vector space in the system described by a $\boldsymbol{k}\cdot\boldsymbol{p}$ Hamiltonian which is the same as Weyl's equation for a neutrino.[21)]

In this paper the conductance is calculated for an impurity with a model potential in a tight-binding model by varying the strength of the potential. The result confirms the absence of back scattering when the potential is sufficiently small, i.e., the maximum value is smaller than the typical width of the conduction and valence bands. When the potential becomes strong, a small probability of back scattering appears. It can be partly explained by higher-order Born scattering in the presence of higher-order terms in $\boldsymbol{k}\cdot\boldsymbol{p}$ perturbations giving rise to a trigonal warping of the bands.[21)] For a sufficiently large potential, the back scattering probability is enhanced resonantly at some specific values of the potential strength and range. In §2, the model and the method of the calculation are discussed. The results are presented in §3. A summary and conclusion are given in §4.

§2. Model and Method

Figure 1 shows the structure of a two-dimensional graphite together with a corresponding Brillouin zone. A unit cell contains two carbon atoms denoted as A and B. The coordinate system (x, y) is chosen in such a way that the x axis is in the chiral direction, i.e., the direction along the circumference or the chiral vector $\boldsymbol{L}$, and the y axis in the direction of the axis. In the following, we consider an armchair nanotube with chiral angle $\eta = -\pi/2$. We use a tight-binding model with a nearest-neighbor hopping integral γ_0 and a lattice constant a.

The armchair nanotube is known to be always metallic and have two bands in the vicinity of the Fermi energy crossing at $k_y = 2\pi/3a$ (K point) and $k_y = -2\pi/3a$ (K' point) as shown in Fig. 2.[22–24)] The dispersion near the Fermi energy is approximately given by $\epsilon = \pm\gamma k$, where k is the wave vector measured from the K and K' point and $\gamma = \sqrt{3}a\gamma_0/2$ with a being the lattice constant. Two channels denoted as K and K' with positive velocity $\gamma/\hbar$ have the dispersion $\epsilon = +\gamma k$ and two with negative velocity $-\gamma/\hbar$ have that of $\epsilon = -\gamma k$.

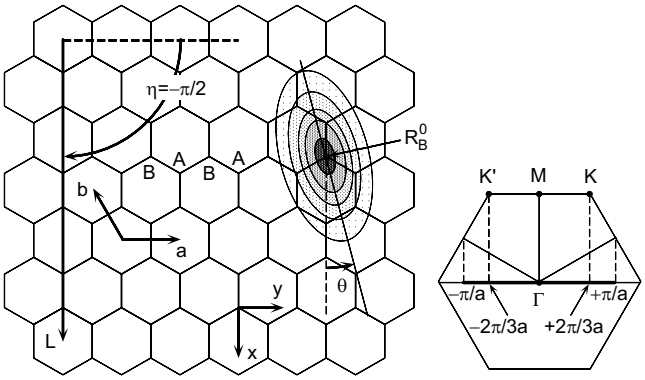

Fig. 1 Schematic illustration of the lattice structure of two-dimensional graphite and the first Brillouin zone. An armchair nanotube is characterized by the chiral vector $\boldsymbol{L}$ and angle $\eta=-\pi/2$ shown in the figure. An impurity with anisotropic Gaussian potential is located at $\boldsymbol{R}_B^0$. The mapping of the corner points K and K' of the first Brillouin zone onto a one-dimensional Brillouin zone is shown also.

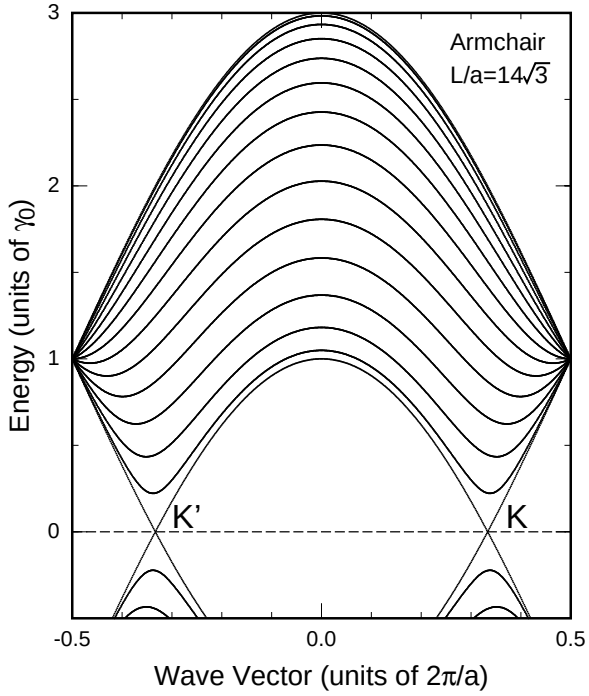

Fig. 2 Calculated band structure of an armchair nanotube with $L/a=14\sqrt{3}$.

We shall calculate a scattering matrix $S=(S_{nm})$, where m and n denote in-coming and out-going channels, respectively. In the vicinity of $\varepsilon=0$, we have two right-going channels $K+$ and $K'+$, and two left-going channels $K-$ and $K'-$. We shall write the scattering matrix as

$$S=\begin{array}{c} \\ K- \\ K'- \\ K+ \\ K'+ \end{array}\!\!\begin{array}{c} \begin{array}{cccc} K+ & K'+ & K- & K'- \end{array} \\ \begin{pmatrix} r_{KK} & r_{KK'} & t'_{KK} & t'_{KK'} \\ r_{K'K} & r_{K'K'} & t'_{K'K} & t'_{K'K'} \\ t_{KK} & t_{KK'} & r'_{KK} & r'_{KK'} \\ t_{K'K} & t_{K'K'} & r'_{K'K} & r'_{K'K'} \end{pmatrix} \end{array}. \tag{2.1}$$

This scattering matrix is calculated numerically using a recursive Green's function technique[25] as in a previous work.[14]

In terms of T matrix defined by

$$T=V+V\frac{1}{\varepsilon-\mathcal{H}_0+\mathrm{i}0}V+V\frac{1}{\varepsilon-\mathcal{H}_0+\mathrm{i}0}V\frac{1}{\varepsilon-\mathcal{H}_0+\mathrm{i}0}V+\cdots, \tag{2.2}$$

with V the impurity potential, ε the energy, and $\mathcal{H}_0$ the Hamiltonian in the absence of an impurity, the scattering matrix can be written formally as

$$S=S^{(0)}+S^{(1)}, \tag{2.3}$$

with

$$S^{(0)}=\begin{pmatrix} 0 & 0 & 1 & 0 \\ 0 & 0 & 0 & 1 \\ 1 & 0 & 0 & 0 \\ 0 & 1 & 0 & 0 \end{pmatrix}, \tag{2.4}$$

and

$$S^{(1)}_{nm}=-\mathrm{i}\frac{A}{\hbar\sqrt{|v_n v_m|}}T_{nm}, \tag{2.5}$$

where A is the length of the nanotube, and v_m and v_n are the velocity of channels m and n.

In the presence of the time reversal symmetry, we have the following relation between the matrix elements of the impurity potential:

$$V_{ab}=(\psi_a^*,V\psi_b)=(\mathrm{e}^{-\mathrm{i}\phi_a}\psi_{\bar{a}},V\mathrm{e}^{\mathrm{i}\phi_b}\psi_{\bar{b}}^*)=\mathrm{e}^{\mathrm{i}(\phi_b-\phi_a)}V_{\bar{b}\bar{a}}, \tag{2.6}$$

where $\psi_{\bar{a}}=\mathrm{e}^{\mathrm{i}\phi_a}\psi_a^*$ and $\psi_{\bar{b}}=\mathrm{e}^{\mathrm{i}\phi_b}\psi_b^*$ are the states obtained from ψ_a and ψ_b, respectively, by the time reversal operation, and ϕ_a and ϕ_b are appropriate phases of the wave function. If we choose the phase such that the eigenfunction for the state $K'-$ is complex conjugate to that for $K+$ and that for $K'+$ is conjugate to $K-$, we can show, using eqs. (2.2) and (2.6),

$$\tilde{S}=\begin{pmatrix} r_1 & r_3 & t_2 & t_4 \\ r_2 & r_1 & t_3 & t_1 \\ t_1 & t_4 & r'_1 & r'_3 \\ t_3 & t_2 & r'_2 & r'_1 \end{pmatrix}, \tag{2.7}$$

where r_1, r_2, r_3, r'_1, r'_2, r'_3, t_1, t_2, t_3, and t_4 should satisfy the unitarity condition $\tilde{S}^+\tilde{S}=\tilde{S}\tilde{S}^+=1$. In general, the scattering matrix can be written in terms of $\tilde{S}$ as

$$S=\begin{pmatrix} \mathrm{e}^{-\mathrm{i}\phi_-} & 0 & 0 & 0 \\ 0 & \mathrm{e}^{-\mathrm{i}\phi'_-} & 0 & 0 \\ 0 & 0 & \mathrm{e}^{-\mathrm{i}\phi_+} & 0 \\ 0 & 0 & 0 & \mathrm{e}^{-\mathrm{i}\phi'_+} \end{pmatrix}\tilde{S}\begin{pmatrix} \mathrm{e}^{\mathrm{i}\phi_+} & 0 & 0 & 0 \\ 0 & \mathrm{e}^{\mathrm{i}\phi'_+} & 0 & 0 \\ 0 & 0 & \mathrm{e}^{\mathrm{i}\phi_-} & 0 \\ 0 & 0 & 0 & \mathrm{e}^{\mathrm{i}\phi'_-} \end{pmatrix}, \tag{2.8}$$

where $\mathrm{e}^{\mathrm{i}\phi_\pm}$ and $\mathrm{e}^{\mathrm{i}\phi'_\pm}$ are determined by the phase of the wave functions. In particular, we have $|r_{KK}|=|r_{K'K'}|$, $|r'_{KK}|=|r'_{K'K'}|$, $t_{KK}=t'_{K'K'}$, $t_{K'K'}=t'_{KK}$, $|t_{KK'}|=|t'_{KK'}|$, and $|t_{K'K}|=|t'_{K'K}|$.

In the Born approximation, we have

$$S^{(1)}_{nm}=-\mathrm{i}\frac{AV_{nm}}{\hbar\sqrt{|v_n v_m|}}. \tag{2.9}$$

Exactly at $\varepsilon=0$, the wave function in the $\boldsymbol{k}\cdot\boldsymbol{p}$ approximation is exact in the absence of an impurity and the matrix element is exactly the same as that given in the

previous paper:[20]

$$V_{K\pm K+} = V_{K'\pm K'+} = \frac{1}{2}(\pm u_A + u_B),$$
$$V_{K\pm K'+} = V^*_{K'\pm K+} = \frac{1}{2}(\mp u'_A e^{i\eta} - \omega^{-1} e^{-i\eta} u'_B), \tag{2.10}$$

with

$$u_A = \frac{\sqrt{3}a^2}{2}\sum_{\boldsymbol{R}_A} V(\boldsymbol{R}_A),$$
$$u'_A = \frac{\sqrt{3}a^2}{2}\sum_{\boldsymbol{R}_A} e^{i(\boldsymbol{K}'-\boldsymbol{K})\cdot\boldsymbol{R}_A} V(\boldsymbol{R}_A),$$
$$u_B = \frac{\sqrt{3}a^2}{2}\sum_{\boldsymbol{R}_B} V(\boldsymbol{R}_B), \tag{2.11}$$
$$u'_B = \frac{\sqrt{3}a^2}{2}\sum_{\boldsymbol{R}_B} e^{i(\boldsymbol{K}'-\boldsymbol{K})\cdot\boldsymbol{R}_B} V(\boldsymbol{R}_B),$$

where $\omega = \exp(2\pi i/3)$, $\sqrt{3}a^2/2$ is the area of a unit cell, and $V(\boldsymbol{R}_A)$ and $V(\boldsymbol{R}_B)$ are the local site energy at $\boldsymbol{R}_A$ and $\boldsymbol{R}_B$, respectively. The above results show that we have $r^*_{K'K} = -r_{KK'}$, $t_{KK} = t_{K'K'}$, $r'^*_{K'K} = -r'_{KK'}$, and $t'_{KK} = t'_{K'K'}$ in the Born approximation.

It should be noted that $|r_{KK'}|$ can be different from $|r_{K'K}|$ in general and the same is true of $|t_{KK}|$ and $|t_{K'K'}|$. In fact, results of numerical calculations presented in the next section show that $|r_{KK'}| \neq |r_{K'K}|$ and $|t_{KK}| \neq |t_{K'K'}|$ for a scatterer with a strong potential.

Depending on the symmetry of the system, we can show various relations among the transmission and reflection coefficients in a manner similar to above in arm chair nanotubes. In the presence of a mirror symmetry around the x axis ($y \to -y$), for example, we have $|t_{K'K}| = |t_{KK'}|$ and $|r_{KK}| = |r'_{KK}| = |r_{K'K'}| = |r'_{K'K'}|$. The same is applicable in the presence of an inversion symmetry around a mid point between neighboring carbon A and B sites. In the presence of a mirror symmetry around the y axis ($x \to -x$), on the other hand, we have $r_{KK} = r_{K'K'} = r'_{KK} = r'_{K'K'} = 0$.[15] We have also $|r_{KK'}(-V)| = |r_{K'K}(V)|$ and $|t_{KK}(-V)| = |t_{K'K'}(V)|$ for arbitrary V, corresponding to the presence of the symmetry of the energy band around $\varepsilon = 0$ in the tight-binding model.

As a model of a scatterer, we consider an anisotropic Gaussian potential with its center at a B site and its range d which is much shorter than the circumference length L. The local site energy is given by

$$V(\boldsymbol{r}) = V_0 \exp\Big[-\frac{(x\cos\theta + y\sin\theta)^2}{(cd)^2} - \frac{(-x\sin\theta + y\cos\theta)^2}{d^2}\Big], \tag{2.12}$$

with the maximum of the potential

$$V_0 = \frac{f(d/a, c)u}{\pi c d^2}, \tag{2.13}$$

where $f(d/a, c)$ is determined by the normalization condition:

$$\sum_{i=A,B}\sum_{\boldsymbol{R}_i} \frac{\sqrt{3}a^2}{4} V(\boldsymbol{R}_i - \boldsymbol{R}^0_B) = u, \tag{2.14}$$

where R_A and R_B are positions of A and B atoms, respectively, $\boldsymbol{R}^0_B$ is the impurity position, and $\sqrt{3}a^2/4$ is the half of the area of a unit cell. An equi-energy line is given by an ellipse whose major axis is rotated from the direction of the x axis by θ. For $c = 1$, eq. (2.12) reduces to an isotropic Gaussian potential used previously.[20]

For the present model impurity potential, we have following relations:

$$u_A + u_B = 2u. \tag{2.15}$$

In the limit of short-range scatterers, i.e., $d \ll a$, we have

$$u_A = 0, \quad u_B = 2u, \quad u'_A = 0, \quad u'_B = 2u. \tag{2.16}$$

In the limit of long-range scatterers, i.e., $d \gg a$, on the other hand, we have

$$u_A = u, \quad u_B = u, \quad u'_A = 0, \quad u'_B = 0. \tag{2.17}$$

Except in the isotropic case $c = 1$, we have $u'_A \neq 0$ because of the absence of symmetry under 120° rotation.

In the conventional $\boldsymbol{k}\cdot\boldsymbol{p}$ scheme, intervalley terms can be neglected and the impurity potential appears only as a diagonal term, when the impurity potential has a range much larger than the lattice constant. The results obtained in this long-range limit within the $\boldsymbol{k}\cdot\boldsymbol{p}$ scheme can be summarized as follows:[20,21] In the lowest order $\boldsymbol{k}\cdot\boldsymbol{p}$ theory neglecting terms of the order of $(ka)^2$, this potential cannot cause back scattering. When a higher order $\boldsymbol{k}\cdot\boldsymbol{p}$ term giving a trigonal warping of the band is included, a weak back scattering appears usually in a higher order Born approximation for $\varepsilon = 0$. For $\varepsilon \neq 0$, back scattering becomes possible even in the lowest order Born approximation except in armchair nanotubes. In an armchair nanotube and for impurity potential having a mirror symmetry about a plane containing the axis of the nanotube, however, the back scattering is not allowed up to an infinite order of Born series.

§3. Numerical Results

In the following calculations, we shall consider a thick nanotube $L/a = 50\sqrt{3}$ and vary the strength of the potential V_0 in the range $-3 < V_0/\gamma_0 < 3$. In the $\boldsymbol{k}\cdot\boldsymbol{p}$ scheme, the strength of the potential is characterized by the parameter $u/\gamma L$.[18] We have

$$\frac{u}{\gamma L} = \frac{2\pi}{\sqrt{3}}\frac{cd^2}{aL}\frac{1}{f(d/a, c)}\frac{V_0}{\gamma_0}, \tag{3.1}$$

which satisfies $|u|/\gamma L \ll 1$ for $d/a \lesssim 1.5$ and $|V_0|/\gamma_0 \lesssim 1$ because $f(d/a, c) \sim 1$ except in the case $d/a \ll 1$. This shows that the lowest Born approximation is always valid in the $\boldsymbol{k}\cdot\boldsymbol{p}$ scheme for this range of the parameters except in some special cases where the lowest term vanishes identically or is extremely small. Therefore, any difference from the Born result obtained in the tight-binding model usually indicates a deviation from the lowest order $\boldsymbol{k}\cdot\boldsymbol{p}$ approximation.

Figure 3 shows the calculated transmission and reflection coefficients for an isotropic scatterer ($c = 1$) as a function of the potential range d/a. In the case of (a) $V_0/\gamma_0 = 0.1$, the difference from the result of the Born approximation is negligible. For a large potential (b)

$V_0/\gamma_0 = 0.5$, on the other hand, the deviation from the Born result becomes appreciable. Higher order effects are important in particular for intervalley terms. Therefore, the potential range necessary for the back scattering to vanish becomes larger with the increase of the potential strength. Due to the mirror symmetry around the x axis the transmission coefficients satisfy the relation $|t_{KK'}| = |t_{K'K}|$. Further, we have approximately $|r_{KK'}| \approx |r_{K'K}|$ (the difference is unrecognizable in the figure).

Figure 4 shows the calculated transmission and reflection coefficients for an anisotropic scatterer ($c=2$ and $\theta = \pi/3$). In the case of (a) $V_0/\gamma_0 = 0.1$, the difference between $|r_{K'K}|$ and $|r_{KK'}|$ remains still very small. For a large potential (b) $V_0/\gamma_0 = 0.5$, both deviation from the Born result and difference between $|r_{K'K}|$ and $|r_{KK'}|$ become appreciable. The absence of back scattering for the range comparable to the lattice constant is destroyed for intervalley terms. Because of the absence of the mirror symmetry, the transmission coefficients $|t_{KK'}|$ and $|t_{K'K}|$ are now different, but the difference remains extremely small.

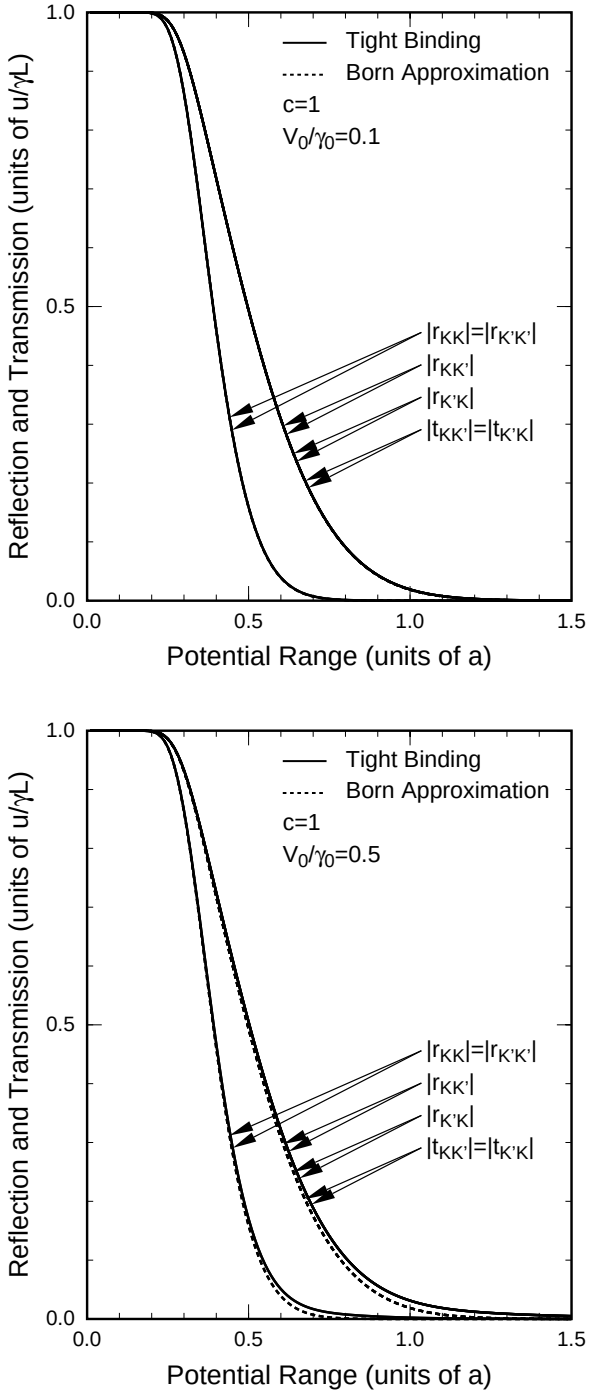

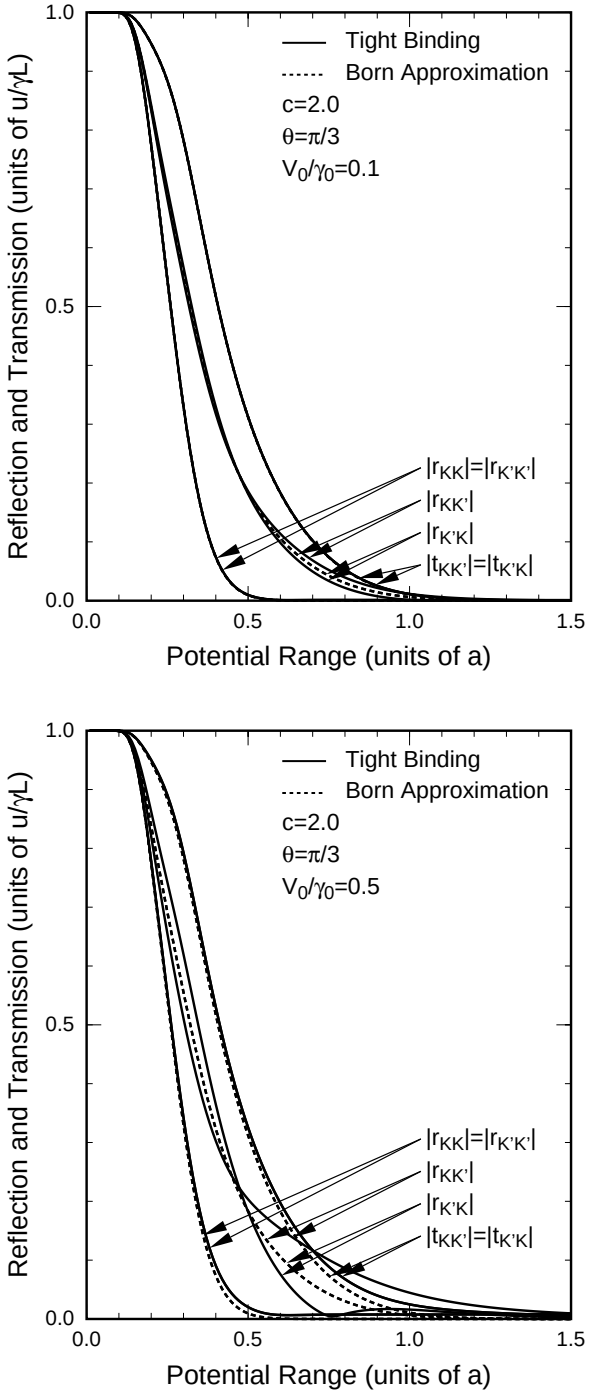

Fig. 3 Calculated transmission and reflection coefficients versus the potential range at $\epsilon = 0$ and for an isotropic scatterer $c = 1$. (a) $V_0/\gamma_0 = 0.1$. (b) $V_0/\gamma_0 = 0.5$.

Fig. 4 Calculated transmission and reflection coefficients versus the potential range at $\epsilon = 0$ for an anisotropic scatterer $c = 2$ and $\theta = \pi/3$. (a) $V_0/\gamma_0 = 0.1$. (b) $V_0/\gamma_0 = 0.5$.

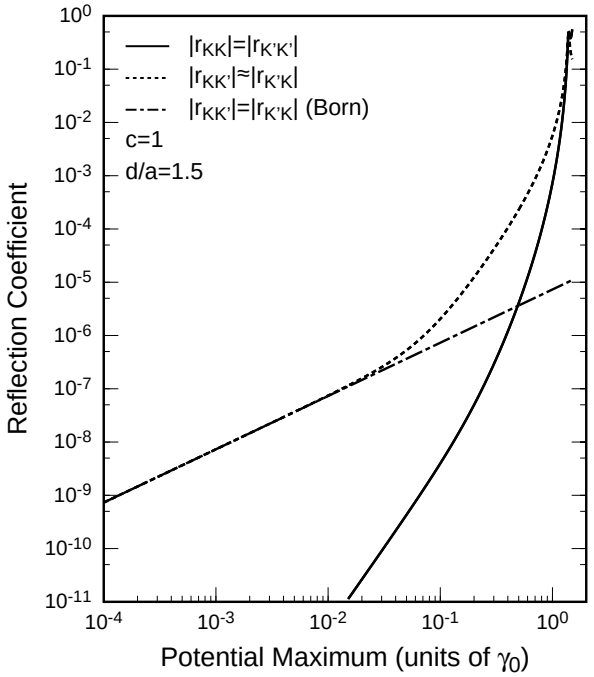

Fig. 5 Calculated reflection coefficients versus the potential strength V_0/γ_0 at $\epsilon = 0$ for an isotropic scatterer ($c=1$) with range $d/a=1.5$.

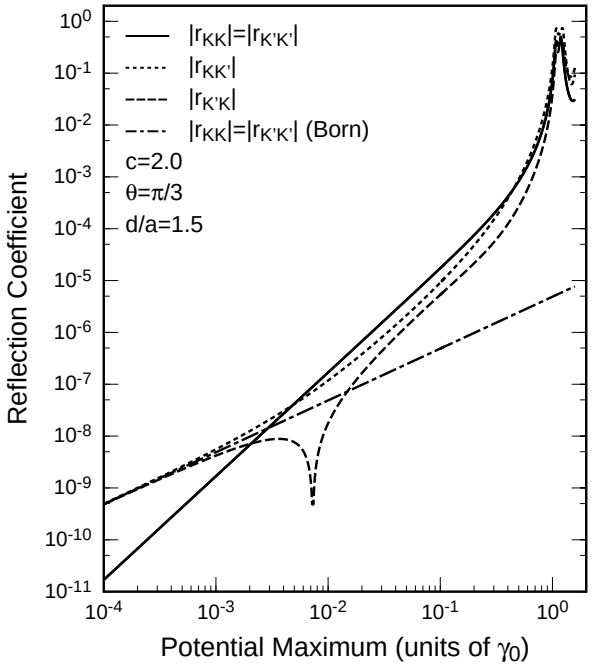

Fig. 6 Calculated reflection coefficients versus the potential strength V_0/γ_0 at $\epsilon=0$ for an anisotropic scatterer ($c=2$ and $\theta=\pi/3$) with range $d/a=1.5$.

Figure 5 shows the calculated reflection coefficients as a function of the potential strength for an isotropic scatterer ($c=1$) with range $d/a=1.5$. For small V_0/γ_0 the intervalley reflection coefficients $|r_{K'K}|$ and $|r_{KK'}|$ increase in proportion to V_0/γ_0 following the lowest Born result, while the intravalley coefficient $|r_{KK}|=|r_{K'K'}|$ is quite small and proportional to $(V_0/\gamma_0)^3$. The origin of this dependence remains to be understood. Higher order effects and therefore the back scattering become appreciable when $V_0/\gamma_0 \gtrsim 0.5$. There seems to be a resonant enhancement of back scattering at a certain potential strength in the region $V_0/\gamma_0 > 1$.

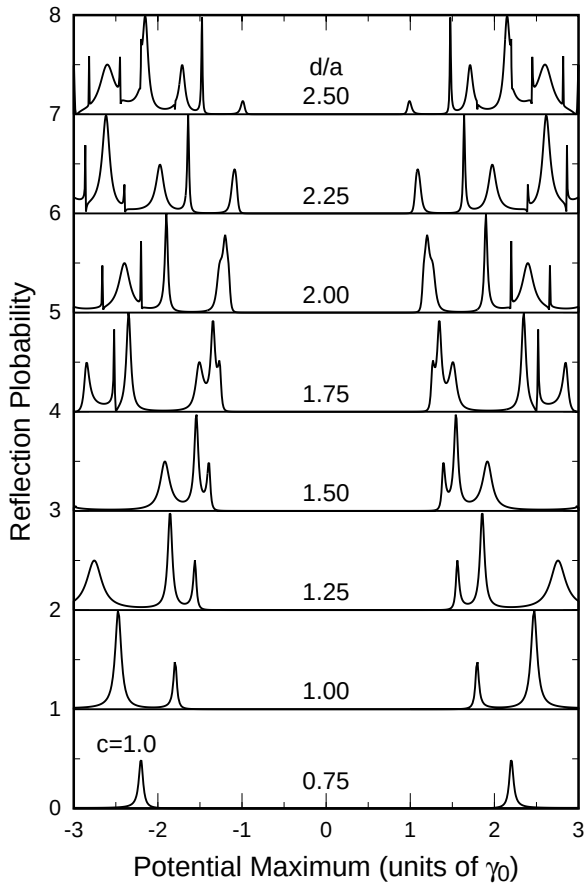

Fig. 7 Calculated total reflection probability of an isotropic scatterer ($c=1$) versus the potential strength V_0/γ_0 at $\epsilon=0$ for various values of the potential range d/a.

Figure 6 shows the calculated reflection coefficients for an anisotropic scatterer ($c=2$ and $\theta=\pi/3$). For small V_0/γ_0 the intervalley coefficients $|r_{K'K}|$ and $|r_{KK'}|$ increase roughly in proportion to V_0/γ_0 following the lowest Born result, but they become different from each other due to higher order effects. Around $V_0/\gamma_0=0.007$, $|r_{K'K}|$ exhibits a sharp dip. This is a result of an interference of the lowest Born term and higher order terms presumably arising from the absence of the mirror symmetry around the y axis combined with higher order $\boldsymbol{k}\cdot\boldsymbol{p}$ terms. The intravalley term $|r_{KK}|=|r_{K'K'}|$ is much larger than that for the isotropic case shown in Fig. 5 and increases in proportion to $(V_0/\gamma_0)^2$. This is a result of the combined effects of higher order terms in the $\boldsymbol{k}\cdot\boldsymbol{p}$ approximation leading to a trigonal warping of the band and higher order Born approximation as mentioned above.

Figure 7 shows the total reflection probability $|r_{K'K}|^2 + |r_{KK'}|^2$ as a function of the absolute value of the potential strength for various values of d/a. The reflection exhibits a complicated resonance behavior when the potential strength exceeds γ_0 and the lowest resonance position approaches $V_0/\gamma_0 = \pm 1$ with the increase of d/a. This shows clearly that this resonance is closely related to the band structure shown in Fig. 2, i.e., the peculiar behaviors at the Brillouin zone edge and center for $\varepsilon/\gamma_0 = \pm 1$. It is likely that some virtual bound states are formed associated with the impurity potential, but

detailed mechanisms remain to be understood yet.

§4. Summary and Conclusion

In summary, we have studied the transmission and reflection coefficient of an armchair CN with a scatterer within a tight-binding model. It has been shown that the result in a $\boldsymbol{k}\cdot\boldsymbol{p}$ scheme is essentially valid unless the strength of the potential becomes comparable to the band width. A small probability of back scattering proportional to the square of potential strength appears for a scatterer with a potential without the mirror symmetry with respect to a line parallel to the tube axis. This is a result of a combination of the trigonal warping of the band arising in higher order $\boldsymbol{k}\cdot\boldsymbol{p}$ perturbations and higher order scattering. When the potential strength is comparable to the band width, a resonant enhancement of back scattering appears presumably due to the peculiar band structure of the two-dimensional graphite.

Acknowledgments

We thank Professor R. Saito for helpful discussions. This work was supported in part by Grant-in-Aid for Scientific Research from Ministry of Education, Science and Culture. One of us (T. N.) acknowledges the support of a fellowship from Special Postdoctoral Researches Program at RIKEN. Numerical calculations were performed in part on FACOM VPP500 in Supercomputer Center, Institute for Solid State Physics, University of Tokyo, and in Institute of Physical and Chemical Research.

1) S. Iijima: Nature (London) **354** (1991) 56.
2) S. Iijima and T. Ichihashi: Nature (London) **363** (1993) 603.
3) D. S. Bethune, C. H. Kiang, M. S. de Vries, G. Gorman, R. Savoy, J. Vazquez, and R. Beyers: Nature (London) **363** (1993) 605.
4) S. N. Song, X. K. Wang, R. P. H. Chang, and J. B. Ketterson: Phys. Rev. Lett. **72** (1994) 697.
5) L. Langer, V. Bayot, E. Grive, J. -P. Issi, J. P. Heremans, C. H. Olk, L. Stockman, C. Van Haesendonck, and Y. Brunseraede: Phys. Rev. Lett. **76** (1996) 479.
6) F. Katayama: Master thesis (Univ. Tokyo, 1996).
7) S. J. Tans, M. H. Devoret, H. -J. Dai, A. Thess, R. E. Smalley, L. J. Geerligs, and C. Dekker: Nature **386** (1997) 474.
8) M. Bockrath, D. H. Cobden, P. L. McEuen, N. G. Chopra, A. Zettl, A. Thess, and R. E. Smalley: Science **275** (1997) 1922.
9) A. Bezryadin, A. R. M. Verschueren, S. J. Tans, and C. Dekker: Phys. Rev. Lett. **80** (1998) 4036.
10) W. -D. Tian and S. Datta: Phys. Rev. B **49** (1994) 5097.
11) R. Saito, G. Dresselhaus, and M. S. Dresselhaus: Phys. Rev. B **53** (1996) 2044.
12) R. Tamura and M. Tsukada: Solid State Commun. **101** (1997) 601.
13) R. Tamura and M. Tsukada: Phys. Rev. B **55** (1997) 4991.
14) T. Nakanishi and T. Ando: J. Phys. Soc. Jpn. **66** (1997) 2973.
15) H. Matsumura and T. Ando: J. Phys. Soc. Jpn. **67** (1998) 3542.
16) Y. Miyamoto, S. G. Louie, and M. L. Cohen: Phys. Rev. Lett. **76** (1996) 2121.
17) T. Seri and T. Ando: J. Phys. Soc. Jpn. **66** (1997) 169.
18) T. Ando and T. Seri: J. Phys. Soc. Jpn. **66** (1997) 3558.
19) N. H. Shon and T. Ando: J. Phys. Soc. Jpn. **67** (1998) 2421.
20) T. Ando and T. Nakanishi: J. Phys. Soc. Jpn. **67** (1998) 1704. There are some typographical errors in this paper. For example, $u_A(\mathbf{R}_A)$ and $u_B(\mathbf{R}_B)$ appearing in the right hand side of eq. (2.18) should be replaced by $\tilde{u}_A(\mathbf{R}_A)$ and $\tilde{u}_B(\mathbf{R}_B)$, respectively.
21) T. Ando, T. Nakanishi, and R. Saito: J. Phys. Soc. Jpn. **67** (1998) 2857.
22) R. Saito, M. Fujita, G. Dresselhaus, and M. S. Dresselhaus: Appl. Phys. Lett. **60** (1992) 2204.
23) N. Hamada, S. Sawada, and A. Oshiyama: Phys. Rev. Lett. **68** (1992) 1579.
24) H. Ajiki and T. Ando: J. Phys. Soc. Jpn. **62** (1993) 1255.
25) T. Ando: Phys. Rev. B **44** (1991) 8017.